ELSEVIER

Journal of Organometallic Chemistry 510 (1996) 219–231

Journal of Organometallic Chemistry

Syntheses, structures and reactivities of $[Os_6Pd(CO)_{18}(bipy)]$ and $[\{(bipy)Pd\}_2Os_3(CO)_{12}]$: crystal and molecular structures of $[\{(bipy)Pd\}_2(\mu\text{-}H)(\mu\text{-}CO)][H_3Os_4(CO)_{12}]$ and $[(C_4H_9)_4N]_2[Pd_2I_6]$

Suzanna Chan [a], Siu-Ming Lee [a], Zhenyang Lin [b], Wing-Tak Wong [a,*]

[a] *Department of Chemistry, The University of Hong Kong, Pokfulam Road, Hong Kong, Hong Kong*

[b] *Department of Chemistry, The Hong Kong University of Science and Technology, Clear Water Bay, Kowloon, Hong Kong*

Received 18 July 1995

Abstract

The complex $[(bipy)Pd(CO_2Me)_2]$ reacts with $[Os_3(CO)_{10}(NCMe)_2]$ in a 1:1 molar ratio to give $[Os_6Pd(CO)_{18}(bipy)]$ (**1**) with a moderate yield, and the crystal structure of **1** is presented. Complex **1** is separately treated with an excess of iodine and tetra-*n*-butylammonium iodide, giving $[Os_6(CO)_{18}]$ and $[(^nBu)_4N]_2[Pd_2I_6]$ (**2**) respectively. Complex **2** is characterized by X-ray crystallography. The cyclic voltammogram of **1** reveals an irreversible oxidation at a potential of around 0.75 V and no reduction wave is observed. On the contrary, the reaction of $[(bipy)Pd(CO_2Me)_2]$ with $[H_2Os_3(CO)_{10}]$ in a 1:2 molar ratio gives $[\{(bipy)Pd\}_2Os_3(CO)_{12}]$ (**3**) with a 25% yield. The X-ray crystallographic study of **3** reveals a stacking situation of the molecules along the *c* axis. Treatment of **3** with an excess of chloride salt leads to the formation of the cationic species $[\{(bipy)Pd\}_2(\mu\text{-}H)(\mu\text{-}CO)]^+$ (**4**) the $[H_3Os_4(CO)_{12}]^-$ salt of which is isolated. Again, a stacking of the dinuclear cations is observed from the X-ray structural analysis of **4**.

Keywords: Osmium; Palladium; Carbonyl; Clusters; Crystal structure

1. Introduction

In recent decades, the chemistry of heterometallic clusters has grown with enormous rate. Numerous bimetallic clusters involving metals in the iron and the nickel triads have been synthesized [1–6]. Yet, an example involving osmium and palladium metal atoms is unknown. The importance of bimetallic platinum alloys in industry [2,7] and the great number of osmium-platinum mixed-metal clusters synthesized arouse our interest in obtaining and investigating the chemistry of stable osmium–palladium clusters. Preliminary reports on the syntheses of two new clusters of the kind $[Os_6Pd(CO)_{18}(bipy)]$ (**1**) [8] and $[\{(bipy)Pd\}_2Os_3(CO)_{12}]$ (**3**) [9] have been published. We now give a full account of their syntheses and some of their chemical reactivities.

2. Results and discussion

2.1. Synthesis of $[Os_6Pd(CO)_{18}(bipy)]$ (1)

The reaction of $[Os_3(CO)_{10}(NCMe)_2]$ with $[(bipy)Pd(CO_2Me)_2]$ in dichloromethane at room temperature does not give many raft clusters $[Os_6(CO)_{21-n}(MeCN)_n]$ ($n = 1, 2$), as is expected from the reactions involving common palladium(II) salts [10] but leads to the formation of the mixed-metal cluster $[Os_6Pd(CO)_{18}(bipy)]$ (**1**) with a moderate yield. In addition to the mentioned species, $[Os_3(CO)_{12}]$ and an uncharacterized brown precipitate were obtained. Complex **1** was isolated in pure form by preparative thin layer chromatography (TLC) on silica. Only terminal carbonyl activity is observed in the carbonyl absorption region of the IR spectrum of **1** in dichloromethane. The proton NMR spectrum recorded in dichloromethane-d_2 confirms the existence of the bipyridine ligand and the absence of any metal hydrides. The mass spectrum confirms the high nuclearity nature of the compound, the molecular ion peak appearing at $m/z = 1908$.

* Corresponding author.

SSDI 0022-328X(95)05901-6

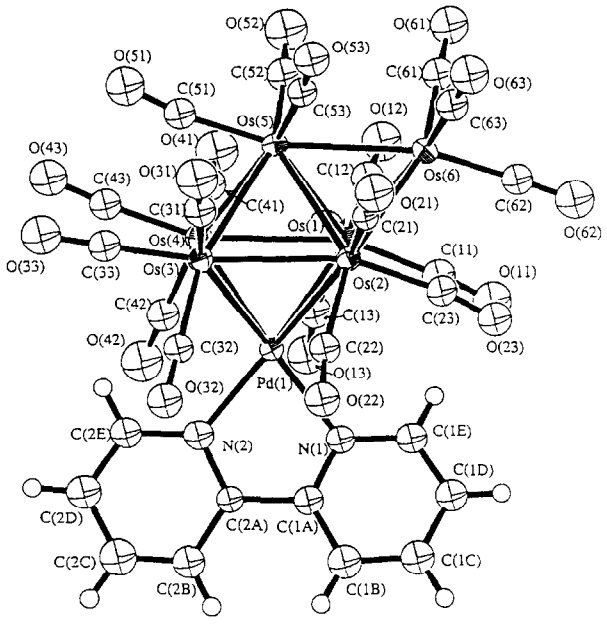

Fig. 1. The molecular structure of $[Os_6Pd(CO)_{18}(bipy)]$ (**1**).

Complex **1** was also obtained as a major product from the reaction of $[Os_6(CO)_{18}]$ with the same palladium reagent. This suggests thermodynamic stability of the compound. No raft-like cluster was formed. Such observation evidences the role of palladium(II) reagents as a coupling reagent for triosmium clusters in the reaction with $[Os_3(CO)_{10}(NCMe)_2]$ only.

The heptanuclear cluster **1** is air stable in the solid state under normal conditions. It dissolves in common polar organic solvents with a high stability. On refluxing in its chloroform solution, it slowly decomposes to give $[Os_6(CO)_{18}]$ and other uncharacterized products.

2.2. Crystal structure of 1

The molecular structure of **1** is depicted in Fig. 1 with the relevant bond distances and angles given in Table 1. The central metal core is analogous to that of the other 98-electron heptanuclear metal clusters [11–17]. Such monocapped octahedral geometry can be rationalized by the polyhedral skeletal electron pair theory [18] and the condensed polyhedral approach [19]. Unlike other six-to-one heterometallic clusters reported [14–17], the heteroatom in **1** occupies the basal apex of the octahedron instead of the capping position. The unsupported Os–Pd bonding distances range from 2.740(2) to 2.808(2) Å while the Os–Os bonding distances range from 2.780(1) to 2.996(1) Å. The four equatorial atoms form a compressed trapezium with the bipyridine plane chopping at the longer sides. In $[Os_7(CO)_{21}]$ [11,12], the capping of the seventh metal atom on the octahedron leads to a shortening effect on the metal–metal bonds of the capped face. The equatorial metal–metal bonds range from 2.834 to 2.892 Å, with the shortest lying along the capped face. On the contrary, such capping effect is overwhelmed by the steric effect imposed by the bipyidine ring in **1**. The latter results in a lengthening of the equatorial sides (2.916(2) Å for the capped side and 2.996(1) Å for the opposite side, cf. an average of 2.828 Å for the others), as well as the bending of the carbonyls on both sides of the ring (Os(1)–C(13)–O(13) = Os(2)–C(22)–O(22) = 166°).

The complex gives a set of multiplets in the range 7.4–9.4 ppm in its ^1H NMR spectrum, which is consistent with the fact that the bipyridine ring on the palladium does not show any fluxional process in the solution state. Thus, from the structural and spectroscopic analyses, we conclude that **1** takes up the same geometric disposition with respect to the bipyridine orientation in both the solid and the solution states.

2.3. Reaction of 1 towards iodine and iodide

Complex **1** was quantitatively converted to $[Os_6(CO)_{18}]$ when an excess of iodine was added to its dichloromethane solution. The solvent was removed in vacuo and a red precipitate was left behind after extrac-

Table 1
Selected bond lengths (Å) and angles (°) for **1**

Bond lengths			
Os(1)–Os(2)	2.916(2)	Os(1)–Os(4)	2.792(1)
Os(1)–Os(5)	2.836(1)	Os(1)–Os(6)	2.813(1)
Os(2)–Os(3)	2.780(1)	Os(2)–Os(5)	2.827(1)
Os(2)–Os(6)	2.803(1)	Os(3)–Os(4)	2.996(1)
Os(3)–Os(5)	2.872(1)	Os(4)–Os(5)	2.872(1)
Os(5)–Os(6)	2.855(1)	Os(1)–Pd(1)	2.791(2)
Os(2)–Pd(1)	2.808(2)	Os(3)–Pd(1)	2.740(2)
Os(4)–Pd(1)	2.790(2)	Pd(1)–N(1)	2.17 (2)
Pd(1)–N(2)	2.15 (3)		
Bond angles			
N(1)–Pd(1)–N(2)	76.2 (7)	Os(1)–C(13)–O(13)	166 (2)
Os(2)–C(22)–O(22)	166 (3)		

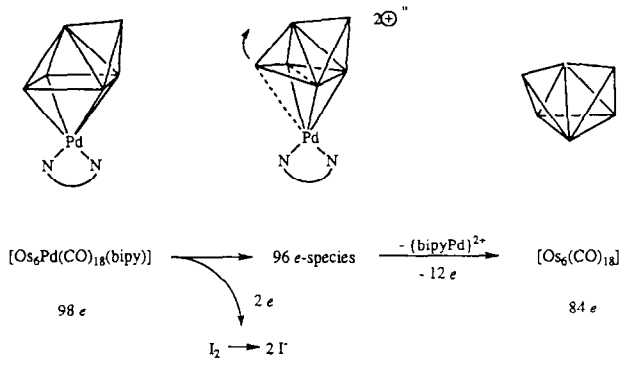

Scheme 1.

Table 2
Selected bond lengths (Å) and angles (°) for **2**

Bond lengths			
Pd(1)–I(1)	2.609(4)	Pd(1)–I(2)	2.594(4)
Pd(1)–I(3)	2.598(4)	Pd(1)–I(4)	2.592(4)
Pd(2)–I(3)	2.600(4)	Pd(2)–I(4)	2.593(4)
Pd(2)–I(5)	2.598(4)	Pd(2)–I(6)	2.594(4)
Bond angles			
I(1)–Pd(1)–I(2)	94.3(1)	I(1)–Pd(1)–I(3)	91.1(1)
I(2)–Pd(1)–I(4)	89.8(1)	I(3)–Pd(1)–I(4)	84.9(1)
I(3)–Pd(2)–I(4)	84.8(1)	I(3)–Pd(2)–I(5)	90.9(1)
I(4)–Pd(2)–I(6)	90.0(1)	I(5)–Pd(2)–I(6)	94.3(1)
Pd(1)–I(3)–Pd(2)	95.0(1)	Pd(1)–I(4)–Pd(2)	95.3(1)

tion of $[Os_6(CO)_{18}]$ by *n*-hexane. The fast atom bombardment (FAB), mass spectroscopy (MS) suggests the red precipitate to be ionic in nature, with the anionic part proposed to be $[Os(CO)_3I_3]^-$. It is the product of the reaction of $[Os_6(CO)_{18}]$ with the excess iodine in the reaction mixture [20]. The cationic part should consist of the {(bipy)Pd} fragment, as indicated from both the positive FAB MS and the proton NMR spectroscopy. A mechanism involving the oxidation of $[Os_6Pd(CO)_{18}$-(bipy)] to a 96-electron species is proposed (Scheme 1).

Fragmentation of the 98-electron cluster is induced by the reduction of iodine. A 96-electron cluster is proposed to be the intermediate, which should adopt a tricapped tetrahedral structure as in $[Au_3CoRu_3(CO)_{12}$-$(PPh_3)_3]$ [21] and $[HAu_3Ru_4(CO)_{12}(PPh_3)_3]$ [22] after a series of skeletal rearrangement. Dissociation of the 12-electron fragment $\{(bipy)Pd\}^{2+}$ from the parent cluster results in the 84-electron complex $[Os_6(CO)_{18}]$.

In contrast, when **1** was reacted with an iodide salt, a mixture of ionic materials was obtained, of which $[(^nBu)_4N]_2[Pd_2I_6]$ (**2**) was isolated as one of the products. The structure was confirmed by X-ray crystallography (Fig. 2 and Table 2), with the same anion as that in the isoquinolium compound previously synthesized [23,24]. The reaction was monitored by IR spectroscopy and TLC. No indication of involvement of $[Os_6(CO)_{18}]$ was observed. The other products reveal carbonyl activity in the IR region but cannot be further characterized.

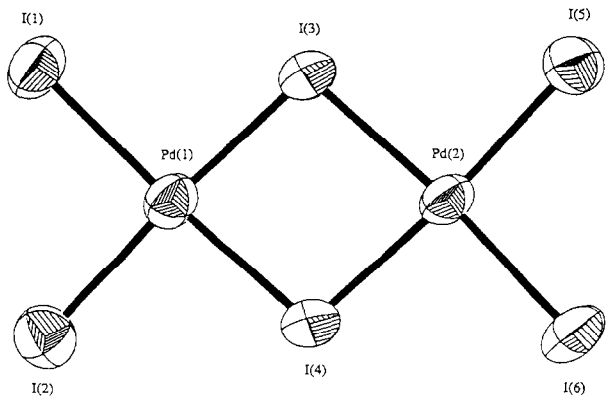

Fig. 2. The molecular structure of $[Pd_2I_6]^{2-}$ (**2**).

2.4. Electrochemistry of 1

In order to rationalize the behaviour of **1** towards the redox reagents, an electrochemical study was carried out. An irreversible-type oxidation potential is noted at around 0.75 V (vs $Ag/AgNO_3$) for **1** at a scan rate of 25 mV s^{-1}, while the reversible oxidation potential of tetra-*n*-butylammonium iodide is at around 0.4 V (vs. $Ag/AgNO_3$). The irreversible oxidation potential of the complex $[(bipy)Pd(CO_2Me)_2]$ is at 0.824 V (vs $Ag/AgNO_3$, 100 mV s^{-1}). The oxidation reaction of **1** with iodine is thus thermodynamically favourable, resulting in structural rearrangement to give $[Os_6(CO)_{18}]$ as the final product. On the contrary, no reduction wave is observed in the cyclic voltammogram of **1**.

2.5. Synthesis of $[\{(bipy)Pd\}_2Os_3(CO)_{12}]$ (3)

When $[H_2Os_3(CO)_{10}]$ was reacted with $[(bipy)Pd(CO_2Me)_2]$ in dichloromethane, $[\{(bipy)Pd\}_2Os_3(CO)_{12}]$ (**3**) was formed as a major product. The red compound was not stable on either silica or alumina plates and was purified by repeated recrystallization. In addition to **3**, $[H_3Os_4(CO)_{12}]^-$ was also formed as the other major product, together with $[H_4Os_4(CO)_{12}]$ and $[Os_3(CO)_{12}]$ as the minor products. Again, no raft-like clusters were produced for the same reason suggested previously to account for the reaction of $[Os_6(CO)_{18}]$ with the palladium complex. Both terminal and bridging carbonyl activities are observed in the IR region. The presence of the bipyridine ligand is confirmed by proton NMR spectroscopy, and again, no fluxional behaviour involving the bipyridine ligand is observed. In order to establish the molecular disposition, a single crystal suitable for X-ray structural analysis was obtained at 0°C from an acetone–chloroform solution of **3**.

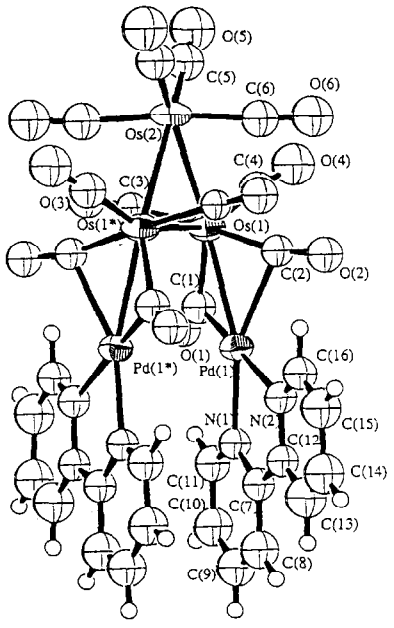

Fig. 3. The molecular structure of $[\{(bipy)Pd\}_2Os_3(CO)_{12}]$ (3).

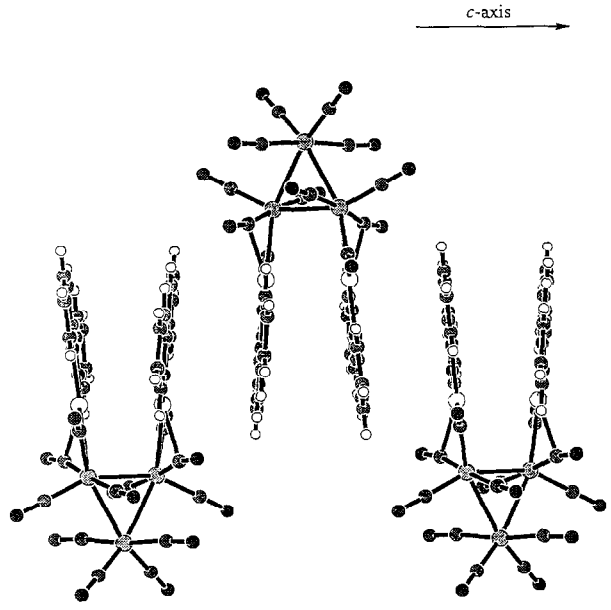

Fig. 4. Projection diagram of 3 along the c axis.

2.6. Crystal structure of 3

The molecular structure of 3 is shown in Fig. 3 with its relevant bonding parameters provided in Table 3. Complex **3** crystallizes in the orthorhombic space group *Fddd*, with the crystallographic two-fold axis passing through the apical osmium. Thus the molecule possesses C_2 symmetry with only half of it composing the asymmetric unit. The five metal atoms adopt a rare open structure [25] which can be described as an isosceles triangle of osmium atoms with two heteroatoms attached to the base in a twisted manner. The palladium-coordinated Os–Os bond is 0.06 Å longer than the other Os–Os bonds (2.851(1) Å). This may be due partly to an electron excess in the osmium atoms and partly to the steric effect imposed by the bipyridine rings. The carbonyl-bridged Os–Pd bond distance is 2.727(1) Å, which is 0.055 Å shorter than the average unsupported Os–Pd bond lengths found in **1**. Such a shortening effect is commonly found in carbonyl-bridged metal–metal bonds due to steric requirements. The two bridging carbonyl ligands adopt different bridging modes: symmetrical and semibridging [26,27]. The situation is similar to that found in $[(bipy)Fe_2(CO)_7]$ [27]. The incipient carbonyl plays the role of reducing the electron density on the osmium. The ligands around the palladium atoms (excluding the osmium atom) take up a distorted square planar geometry, with the incipient bridging carbonyl ligand bending out of the plane. The large difference in the Pd–N bond lengths of the bipyridine ligand directly reflects the greater *trans* influence of the symmetrical bridging carbonyl compared with the semibridging carbonyl. The bonding environment around the palladium atom has been further investigated by molecular orbital calculations (vide infra).

Fig. 4 illustrates the stacking picture of **3** along the crystallographic *c* axis. The intrinsic C_2-symmetric na-

Table 3
Selected bond lengths (Å) and angles (°) for **3**

Bond lengths			
Os(1)–Os(1*)	2.912(1)	Os(1)–Os(2)	2.851(1)
Os(1)–Pd(1)	2.727(1)	Pd(1)···Pd(1*)	2.973(2)
Os(1)–C(1)	2.02 (2)	Os(1)–C(2)	1.96 (2)
Pd(1)–C(1)	1.98 (2)	Pd(1)–C(2)	2.34 (2)
Pd(1)–N(1)	2.18 (1)	Pd(1)–N(2)	2.26 (1)
Bond angles			
Os(1*)–Os(1)–Os(2)	59.3 (1)	Os(1)–Os(2)–Os(1*)	61.4 (1)
Os(1*)–Os(1)–Pd(1)	86.1 (1)	Os(2)–Os(1)–Pd(1)	141.9 (1)
Os(1)–C(1)–O(1)	144 (1)	Os(1)–C(2)–O(2)	167 (1)
Pd(1)–C(1)–O(1)	129 (1)	Pd(1)–C(2)–O(2)	113 (1)
Os(1)–C(1)–Pd(1)	86.1 (7)	Os(1)–C(2)–Pd(1)	78.2 (6)
N(1)–Pd(1)–N(2)	75.6 (5)	C(1)–Pd(1)–C(2)	87.8 (6)

ture of the molecule causes a rotation of 45° about the Pd–Pd axis for the intramolecular bipyridine rings. The whole molecule rotates by 180° about the midpoint of the projection vector of Pd(1)–C(8) on the a–b plane for a consecutive molecule in the stack. The combined effect relieves the steric hindrance imposed. The intramolecular and intermolecular separations of the rings (3.45 and 3.49 Å respectively) suggest the involvement of π–π interaction [28–30] in the lattice.

2.7. Molecular orbital calculations for 3

The cluster has a total number of 76 valence electrons involved in the metal–metal and metal–ligand interactions. Formally, there is no Pd · · · Pd bond if one assumes palladium conforming to a 16-electron rule and osmium to an 18-electron rule. The assumption is reasonable because the local coordination structure of each palladium is approximately planar. For a metal complex with planar structure, the p_z orbital (the z axis is perpendicular to the molecular plane) is normally unoccupied.

To study the metal–metal and metal–ligand interactions in the cluster, both Fenske–Hall and the extended Hückel molecular orbital (EHMO) calculations were performed. The Mulliken overlap populations (bond orders) are shown in Figs. 5(a) and 5(b) for the metal–metal and Pd–ligand interactions respectively. Both the Fenske–Hall and the EHMO calculations give similar atom–atom overlap populations. The Pd · · · Pd bond order is relatively small. The Fenske–Hall method gives slightly negative while the EHMO gives slightly positive results. This indicates that the Pd · · · Pd interaction is insignificant, and therefore supports the conclusion derived from the formal electron counting mentioned above. Both calculations give a positive Os–Pd overlap population although it is very small. This may indicate that there is a weak Pd → Os dative bond, which will be discussed below.

Of the two Pd–CO bonds, one bond is significantly weaker than the other (see overlap populations in Fig. 5(b)). This carbonyl ligand is considered semibridging because the Os–C–O angle is 167°. The two Pd–N overlap populations are almost the same. To examine

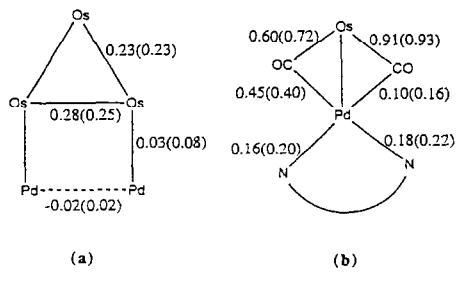

Fig. 5. Diagram showing the Mulliken overlap populations of 3 for (a) the metal–metal interaction and (b) the Pd–ligand interaction.

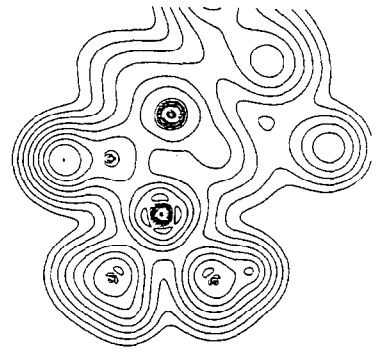

Fig. 6. The total electron density contour of 3 around Pd(1).

the detailed electron distribution around each Pd centre, a total density contour display is shown in Fig. 6 on the plane containing approximately all the ligand atoms bonded to the Pd centre. It can be seen from Fig. 6 that the two NH_3 ligands (see Section 3) and the bridging CO on the left-hand side of the figure are bonded to the palladium through the electron depletions around the central atom, as usual for ligand → metal dative bonds [31]. One maximum around the palladium centre is in the direction of Os · · · Pd and the other is towards the semibridging CO. Therefore, the Os · · · Pd interaction can be formally taken as a weak Pd → Os dative bond. Based on these arguments, we can provide a formal bonding description around the palladium centre, shown in Fig. 7. In the Pd–ligand plane, the palladium atom uses its two d electron pairs (d_{xy} and $d_{x^2-y^2}$ if the z axis is perpendicular to the molecular plane), forming two dative bonds with the osmium and the semibridging carbonyl group. It should be noted here that Fig. 7 provides only an intuitive picture.

2.8. Reaction of 3 with chloride

To an acetone solution of **3**, an excess of a chloride salt was added. A dark-red fibrous product precipitated out, giving a pale-yellow filtrate. The filtrate was decanted after centrifuge. A bright-red solution of $[\{(bipy)Pd\}_2(\mu\text{-}H)(\mu\text{-}H)(\mu\text{-}CO)]^+$ (**4**) was obtained on extraction of the residue with methanol. Gradual addition of n-hexane precipitated **4** out as its $[H_3Os_4(CO)_{12}]^-$ salt in an orange–yellow fibrous form. The compound in methanol solution slowly decomposed in air over a few days, giving some insoluble black precip-

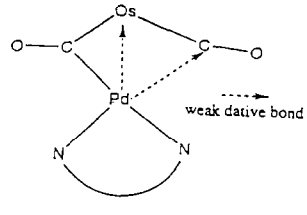

Fig. 7. Formal bonding descriptive picture around Pd(1) for 3.

itate. Besides the terminal carbonyl activity of the anion, the IR spectrum of **4** reveals some bridging carbonyl activity at 1795 cm^{-1} (KBr disc). The ^1H NMR signals at 7.3–9.0 ppm are ascribed to the bipyridine protons and a metal hydride resonance signal occurs at −14.66 ppm. The signal is much more up-field than in $[(Ph_3P)_4Pd_2(\mu\text{-}H)(\mu\text{-}CO)]^+$ [32,33] and $[\{(dippp)Pd\}_2(\mu\text{-}H)(\mu\text{-}CO)]^+$ [34,35], owing to the higher electron density on the palladium atoms. Rapid proton exchange accounts for the absence of the hydride signals of the anion. The molecular configuration is established by X-ray structural analysis on a red single crystal obtained from a methanol–acetone solution of the cluster salt of **4** at 0°C overnight.

It is believed that the attack of the chloride ion on **3** results in the breaking of the Os–Pd bonds, as in the reaction of **1** with iodide. The combined effect of coordination to the Os–Os edge and the π–π interaction of the bipyridine rings bring the palladium atoms to close proximity, so that coupling of the two {(bipy)Pd} fragments occurs instead of complete decomposition (cf. **1**). Carbonyl rearrangement and the abstraction of a proton from the solvent result in the formation of **4**, which is stabilized by the presence of the counterion. The latter is generated from the osmium remains of **3**. The yield of **4** was increased if the reaction was carried out on an acetone extract of **3** obtained from its synthesis in situ. This may be accounted for by the intrinsic presence of $[H_3Os_4(CO)_{12}]^-$ in the reaction mixture, stabilizing the formation of the cation.

2.9. Crystal structure of 4

An ORTEP plot of **4** is shown in Fig. 8, with the relevant bond lengths and bond angles listed in Table 4. The structure is analogous to that of $[\{(dippp)Pd\}_2(\mu\text{-}H)(\mu\text{-}CO)]^+$ [34,35]. It consists of two {(bipy)Pd} fragments fused together, with a hydride and a carbonyl ligand bridging on the opposite sides of the Pd(I)–Pd(I) bond [36,37]. A formal Pd(I)–Pd(I) bond is assigned from the electron count of the metal centres, with a

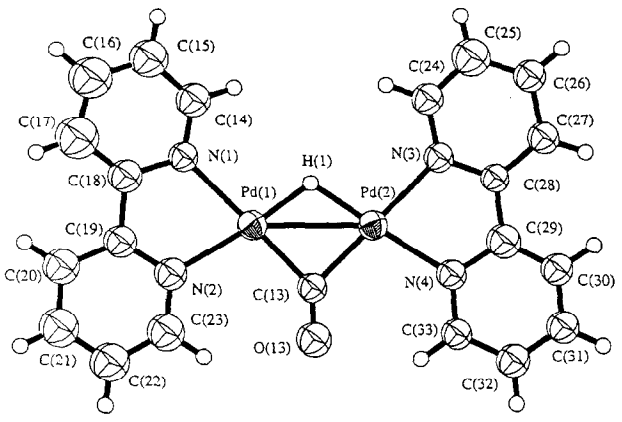

Fig. 8. The molecular structure of $[\{(bipy)Pd\}_2(\mu\text{-}H)(\mu\text{-}CO)]^+$ (**4**).

bonding distance of 2.691(3) Å (vide infra). The shorter Pd–Pd distance compared with $[\{(dippp)Pd\}_2(\mu\text{-}H)(\mu\text{-}CO)]^+$ (2.767 Å) is a direct outcome of the replacement of π-acid ligands by better σ-donating ligands, strengthening the bonds with the corresponding bridging carbonyl ligands. The $\{Pd_2(H)(CO)\}$ fragment lies in a planar fashion, with the two bipyridine ligands bending out of the plane in an opposite manner. The dihedral angles between each bipyridine ligand and the $Pd_2(H)(CO)$ plane are 8.89 and 1.41°. The two pyridine rings of each bipyridine ligand are twisted along the C–C bond with dihedral angles of 5.93 and 5.99°. Again, the ligands are coordinated to each palladium atom in a distorted square planar geometry, with a dihedral angle of 3.7° between the two planes. A comparatively small *trans* influence is observed with the Pd–N bonds opposite to the bridging carbonyl slightly longer than that opposing the hydride (cf. **3**).

Fig. 9 shows the packing diagram of the cation with the Pd–Pd distances as labelled. Stacking of the bipyridine rings along the *c* axis persists throughout the lattice. The cations align in a paired manner, with consecutive cations lying in an opposite direction with respect to the bridging carbonyl. A small degree of

Table 4
Selected bond lengths (Å) and angles (°) for **4**

Bond lengths			
Pd(1)–Pd(2)	2.691(3)	Pd(1)–Pd(1′)	3.230(4)
Pd(1)–Pd(2′)	3.416(3)	Pd(2)–Pd(2″)	3.435(4)
Pd(1)–C(13)	1.94 (2)	Pd(1)–H(1)	1.64
Pd(1)–N(1)	2.17 (2)	Pd(1)–N(2)	2.12 (2)
Pd(2)–C(13)	1.96 (2)	Pd(2)–H(1)	1.68
Pd(2)–N(3)	2.15 (2)	Pd(2)–N(4)	2.09 (2)
C(13)–O(13)	1.17 (2)		
Bond angles			
N(1)–Pd(1)–N(2)	76.7 (8)	C(13)–Pd(1)–H(1)	82.9
N(3)–Pd(2)–N(4)	78.1 (7)	C(13)–Pd(2)–H(1)	81.3
Pd(1)–C(13)–Pd(2)	87 (1)	Pd(1)–C(13)–O(13)	137 (1)
Pd(1)–H(1)–Pd(2)	108		

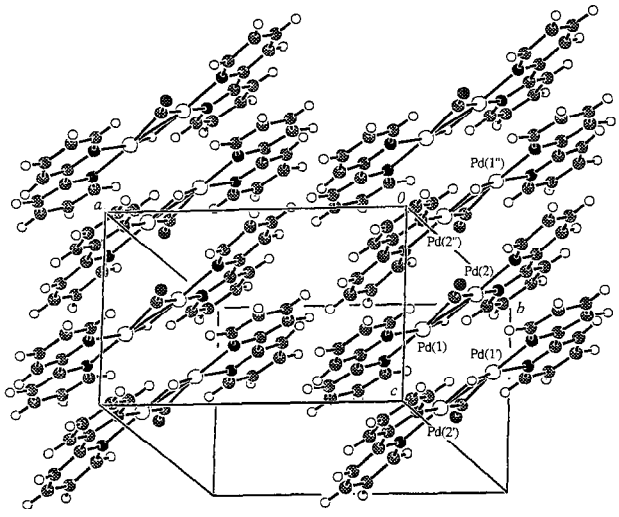

Fig. 9. Unit cell packing diagram of 4. The Pd–Pd distances are as follows: Pd(1)–Pd(1'), 3.23 Å; Pd(1)–Pd(2'), 3.42 Å; Pd(1)–Pd(1"), 7.21 Å; Pd(1)–Pd(2"), 4.97 Å; Pd(2)–Pd(2'), 5.23 Å; Pd(2)–Pd(2"), 3.43 Å.

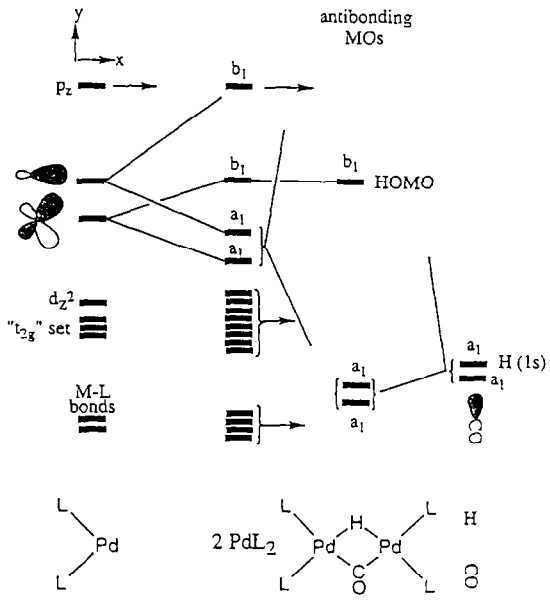

Fig. 10. The orbital interaction diagram of $[L_2Pd(\mu\text{-}CO)(\mu\text{-}H)PdL_2]$: MO, molecular orbital; HOMO, highest occupied molecular orbital.

lateral displacement can be observed for every alternate cation. Such slippage together with the rotation of the cation relieve the steric repulsion of the rings. The interionic Pd–Pd distances range from 3.23 to 7.21 Å (Fig. 9). Such close proximity is believed to be brought about by the π–π interaction of the bipyridine ligands [28–30]. Interaction is expected but no formal Pd–Pd bond is assigned to the intermolecular palladium atoms.

2.10. Molecular orbital calculations of 4

The cluster has a total number of 30 valence electrons involved in the metal–metal and metal–ligand interactions. Formally, there is one Pd · · · Pd bond if one assumes Pd conforming to a 16-electron rule since the local coordination structure of each Pd is approximately planar.

To study the metal–metal and metal–ligand interactions in the cluster, a Fenske–Hall molecular orbital calculation was performed. The Mulliken overlap populations (bond orders) of Pd–CO, Pd–H and Pd–N are 0.53, 0.32 and 0.23 respectively. Surprisingly, the Pd · · · Pd bond order is negligibly negative (−0.03) although the formal electron counting gives a metal–metal bond. This result implies that the direct Pd · · · Pd interaction is small and that the Pd · · · Pd interaction may occur through the bridging ligands. To appreciate this indirect interaction, we examine the molecular orbitals from the Fenske–Hall calculations in detail. A schematic orbital interaction diagram can be constructed from the detailed molecular orbital analyses. Fig. 10 shows the PdL_2 fragment orbital energy levels and the orbital interactions of $[L_2Pd(\mu\text{-}CO)(\mu\text{-}H)PdL_2]$ derived from two PdL_2 fragments and the bridging ligands. For theoretical simplification, only metal–ligand σ interactions are shown in the figure. In PdL_2, the fragment orbitals span as two Pd–L σ bonds, "t_{2g}" set, d_{z^2}, two frontier orbitals and p_z (see the column in the left-hand

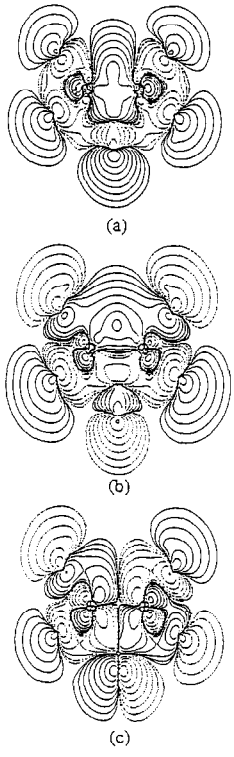

Fig. 11. (a) The Pd · · · Pd σ bonding wavefunction, (b) the Pd · · · Pd π bonding wavefunction and (c) the Pd · · · Pd π antibonding wavefunction of $[L_2Pd(\mu\text{-}CO)(\mu\text{-}H)PdL_2]$.

side in Fig. 10). The p_z orbital is too high in energy to be available for metal–metal or metal–ligand interaction. The interactions among the "t_{2g}" sets and d_{z^2} orbitals lead to half in-phase combinations and half out-of-phase combinations. These orbitals are all occupied and therefore do not contribute to the direct Pd · · · Pd bonding. It can be seen from Fig. 10 that the molecular orbitals, which have effective bonding within the {Pd(μ-CO)(μ-H)Pd} unit, are the three orbitals ($a_1 + a_1 + b_1$) shown in the third column of Fig. 10. The wavefunctions of these three molecular orbitals are plotted in Fig. 11. The two a_1 shown in Figs. 11(a) and 11(b) are the bonding orbitals. Fig. 11(a) is a Pd · · · Pd σ bonding wavefunction and shows no significant contours along the Pd · · · Pd bond. Fig. 11(b) is a Pd · · · Pd π bonding wavefunction while Fig. 11(c) is a Pd · · · Pd π antibonding wavefunction. The π antibonding orbital (the highest occupied molecular orbital) is significantly stabilized by the π* of the bridging CO. The occupation of these three orbitals does not lead to a significant Pd · · · Pd direct interaction. Therefore, the Mulliken analysis shows a negligible Pd · · · Pd overlap population. The net bond derived from the formal electron counting, in fact, is from the a_1 shown in Fig. 11(a). This net bond is delocalized in the Pd–H–Pd three centres.

3. Experimental details

3.1. Materials and methods

All the reactions were performed under an atmosphere of dry dinitrogen using Schlenk-type apparatus. The solvents were purified and dried by conventional methods. The compounds $[Os_3(CO)_{10}(NCMe)_2]$, $[H_2Os_3(CO)_{10}]$, $[Os_6(CO)_{18}]$ and $[(bipy)Pd(CO_2Me)_2]$ were prepared according to the reported syntheses [38,39]. Other chemicals were obtained from commercial sources. IR spectra were recorded on a BIO-RAD FTS-7 IR spectrometer, using 0.5 mm calcium fluoride solution cells. The NMR spectra were recorded on a JEOL GSX 270FT-NMR spectrometer with $SiMe_4$ as the internal reference. Mass spectra were recorded on a Finnigan MAT 95 instrument with the FAB technique. Plates coated with Merck Kieselgel 60 GF_{254} were used for thin layer chromatography separation of the products.

All electrochemical measurements were carried out under a nitrogen purge to exclude oxygen. Dichloromethane, distilled over calcium hydride, was deoxygenated prior to use. The supporting electrolyte was 0.1 M tetra-*n*-butylammonium tetrafluoroborate (Janssen Chimica) in CH_2Cl_2. Voltammetric experiments were performed with a Princeton Applied Research (PAR) model 273A potentiostat, connected to an interfaced computer. A standard three-electrode cell consisting of an $Ag/AgNO_3$ reference electrode (Bioanalytical), a platinum wire counterelectrode (Aldrich) and a glassy carbon working electrode (Bioanalytical) was employed. Positive feedback *iR* compensation was applied as usual.

3.2. Synthesis of $[Os_6Pd(CO)_{18}(bipy)]$ (1)

A solution of $[Os_3(CO)_{10}(NCMe)_2]$ (20 mg, 0.021 mmol) was stirred with $[(bipy)Pd(CO_2Me)_2]$ (8 mg, 0.021 mmol) in CH_2Cl_2 (20 ml) at ambient temperature for 2 h. After reduction in the volume, the filtrate was separated by preparative TLC on silica, with an eluent of *n*-hexane: CH_2Cl_2 (7:3 v/v). Complex **1** was isolated as the major product ($R_f = 0.3$) with a 25% yield (8 mg). IR (CH_2Cl_2): ν(CO) 2091w, 2056s, 2047s, 2026m, 2016m, 1984w cm^{-1}. ^1H NMR (CD_2Cl_2): δ 9.33 (dt, 1H), 8.13 (m, 4H), 7.99 (td, 1H), 7.80 (m, 1H), 7.39 (m, 1H) ppm. FAB MS (+ve): *m/z* 1908 (1908 simulated).

Complex **1** was also obtained with a 48% yield (11 mg) from the reaction of $[Os_6(CO)_{18}]$ (20 mg, 0.012 mmol) with $[(bipy)Pd(CO_2Me)_2]$ (4.6 mg, 0.012 mmol).

3.3. Reaction of 1 with iodine

10 mg of **1** (0.005 mmol) was dissolved in CH_2Cl_2 (10 ml). A twentyfold excess of iodine (26.6 mg) dissolved in CH_2Cl_2 (10 ml) was gradually introduced to the solution at room temperature over 1/2 h. The mixture was stirred for a further 1/2 h after all the starting material had been converted to $[Os_6(CO)_{18}]$, as indicated by both IR spectroscopy and thin plate chromatography on silica. The mixture was dried in vacuo. $[Os_6(CO)_{18}]$ was extracted by *n*-hexane in air, leaving a bright-red residue which contains the $[Os(CO)_3I_3]^-$ anion.

3.4. Reaction of 1 with iodide

A mixture of **1** (10 mg, 0.005 mmol) and a tenfold excess of tetra-*n*-butylammonium iodide (19 mg, 0.051 mmol) was stirred in CH_2Cl_2 (20 ml) for 1 h at room temperature. The mixture was then separated by preparative TLC with CH_2Cl_2: *n*-hexane (6:4 v/v) as eluent, giving four bands of similar abundance with $R_f < 0.3$. Crystalline material of $[(^nBu)_4N]_2[Pd_2I_6]$ (**2**) was obtained from the extract of the dark-red band with $R_f = 0.2$. Slow evaporation of a CH_2Cl_2–*n*-hexane solution in air gave single crystals of **2** which were suitable for X-ray analysis.

3.5. Synthesis of $[\{(bipy)Pd\}_2Os_3(CO)_{12}]$ (3)

Addition of a CH_2Cl_2 solution of $[(bipy)Pd(CO_2Me)_2]$ (18 mg, 0.04 mmol) to $[H_2Os_3(CO)_{10}]$ (20

Table 5
Crystallographic data and data collection parameters for **1–4**

Compound	$[Os_6Pd(CO)_{18}(bipy)]\cdot CHCl_3$ (**1**)	$[^nBu_4N]_2[Pd_2I_6]$ (**2**)	$[\{(bipy)Pd\}_2Os_3(CO)_{12}]$ (**3**)	$[\{(bipy)Pd\}_2(\mu\text{-}H)(\mu\text{-}CO)]^+[H_3Os_4(CO)_{12}]^-$ (**4**)
Empirical formula	$C_{29}Cl_3H_9N_2O_{18}Os_6Pd$	$C_{32}H_{72}I_6N_2Pd_2$	$C_{32}H_{16}N_4O_{12}Os_3Pd_2$	$C_{33}H_{20}N_4O_{13}Os_4Pd_2$
Formula weight	2027.36	1459.16	1431.90	1654.14
Colour, habit	Dark-red plate	Red square plate	Bright-red rod	Fine orange rod
Crystal size (mm)	0.18×0.32×0.32	0.05×0.30×0.30	0.15×0.15×0.32	0.08×0.08×0.25
Crystal system	Triclinic	Monoclinic	Orthorhombic	Triclinic
Space group	$P\bar{1}$ (No. 2)	$P2_1/c$ (No. 14)	$Fddd$ (No. 70)	$P\bar{1}$ (No. 2)
Number of reflections used for cell determination	25	25	20	14
a (Å)	10.041(1)	14.586(6)	29.838(10)	13.938(5)
b (Å)	11.409(6)	14.111(5)	39.614(7)	18.497(6)
c (Å)	17.076(5)	24.021(7)	13.469(3)	8.241(2)
α (°)	97.89(3)	90	90	100.37(3)
β (°)	93.89(2)	100.87(4)	90	100.08(3)
γ (°)	91.04(2)	90	90	70.11(2)
Volume (Å^3)	1933(5)	4855(3)	15920(15)	1950(1)
Z	2	4	16	2
D_{calc} (g cm^{-3})	3.475	1.996	2.389	2.817
μ(Mo Kα)(cm^{-1})	204.23	45.79	104.84	139.40
F(000)	1788	2752	10432	1492
Temperature (K)	293	298	298	298
Scan type	ω–2θ	ω–2θ	ω–2θ	ω–2θ
Scan rate in ω (° min^{-1})	1.03–16.48	16.0 (up to 4 scans)	16.0 (up to 4 scans)	16.0 (up to 4 scans)
Scan range (°)	0.50 + 0.34 tan θ	0.73 + 0.35 tan θ	1.26 + 0.35 tan θ	0.68 + 0.35 tan θ
Maximum 2θ (°)	45.0	45.0	45.0	45.0
Transmission factor	0.3549–1.0000	0.6616–1.0000	0.6462–1.0000	0.9049–1.0000
Number of reflections collected	5724	6982	2856	5335
Number of unique reflections	5046	6676	2856	5082
Number of observed reflections ($F > n\sigma(F)$)	3678 ($n = 3$)	2317 ($n = 6$)	1515 ($n = 6$)	2260 ($n = 6$)
Direct method for solution	MULTAN 80	SAPI 90	SIR 88	SAPI 91
Weighting scheme $w = 4F_o^2/[\sigma^2(F_o^2) + g(F_o^2)^2]$	$g = 0.04$	$g = 0.005$	$g = 0.002$	$g = 0.014$
R	0.041	0.063	0.031	0.036
R_w	0.067	0.063	0.028	0.034
Goodness of fit	1.93	2.63	1.55	1.15
Largest Δ/σ	0.03	0.00	0.00	0.00
Number of parameters	287	209	120	255
Residual electron density (electrons Å^{-3})	1.51 to (−2.58) close to Os	1.36 to (−1.88) close to Pd or I	0.88 to (−0.63)	0.92 to (−0.79)

mg, 0.023 mmol) in the same solvent gave an orange–red suspension. The IR spectrum of the filtrate confirmed the presence of $[H_3Os_4(CO)_{12}]^-$ [40] as the major product. The solvent was removed in vacuo and the residue was extracted with small portions of CH_2Cl_2 (2 × 5ml). The filtrate on separation by TLC (CH_2Cl_2: *n*-hexane, 3:7 v/v) gave $[Os_3(CO)_{12}]$ as the minor product. The majority of the mixture, staying at the baseline of the plate, was found to be the anionic cluster mentioned above. The residue was extracted with acetone (10 ml) to give a bright-red solution. Red crystalline material of **3** was obtained on keeping the concentrated solution at 0°C overnight, (yield, 8 mg (25%)). IR (CH_2Cl_2): ν(CO) 2081w, 2068m, 2035s, 2020s, 1998s, 1798br w cm^{-1}. ^1H NMR (acetone-d_6): δ 9.14 (m, 1H), 8.49 (m, 2H), 8.30 (m, 1H), 8.06 (m, 2H), 7.92 (m, 1H), 7.57 (m, 1H) ppm. FAB MS (-ve): m/z 1431 (1432 simulated).

3.6. Reaction of 3 with chloride

To an acetone solution (15 ml) of **3** (20 mg, 0.014 mmol), a 5 ml acetone solution of tetraethylammonium chloride (7 mg, 0.042 mmol) was added with stirring. A dark red fibrous material was precipitated immediately. After centrifuge, the filtrate was decanted and was identified to be $[H_3Os_4(CO)_{12}]^-$ major by IR spectroscopy. The residue was extracted with methanol to give a bright-red solution. The orange–yellow fibrous form of **4** (40% yield), with $[H_3Os_4(CO)_{12}]^-$ as the counterion, was obtained on dropwise addition of *n*-hexane. The yield of **4** was improved to 55% by using an impure acetone extract of **3** obtained from it synthesis in situ. Spectroscopic data of **4** was as follows. IR (KBr): ν(CO) 2040m, 2016m, 1994m, 1795br s cm^{-1}. ^1H NMR (methanol-d_4): δ 8.99 (m, 2H), 8.35 (m, 2H), 7.83 (m, 8H), 7.37 (m, 4H), −14.66 (s, 1H) ppm. FAB MS: m/z 551 (+ve, 555 simulated), 1102 (-ve, 1101 simulated).

3.7. Molecular orbital calculations for 3 and 4

Molecular orbital calculations were performed within both the Fenske–Hall [41] and the extended Hückel [42] methods for **3** and the former only for **4**. The NH_3 ligands were used to model the bipyridine ligands in the clusters. The geometrical parameters were taken from the X-ray crystal structures described in this paper. In the Fenske–Hall calculations, the basis functions were generated by a method described in the literature [41b]. In the EHMO calculation, parameters of all non-metal atoms were taken from the literature [43]. For the Os atoms, $H_{ii}(s) = -8.0$ eV, $\zeta(s) = 2.14$; $H_{ii}(p) = -4.5$ eV, $\zeta(p) = 2.1$; $H_{ii}(d) = -12.5$ eV, $\zeta_1(d) = 4.29$ ($c_1 = 0.5935$) and $\zeta_2(d) = 1.97$ ($c_2 = 0.5835$). For the Pd atoms, $H_{ii}(s) = -7.32$ eV, $\zeta(s) = 2.19$; $H_{ii}(p) = -3.75$

Table 6
Atomic coordinates for **1** with estimated standard deviations in parentheses

Atom	*x*	*y*	*z*
Os(1)	0.46211(8)	0.36260(8)	0.27241(5)
Os(2)	0.17485(7)	0.36568(7)	0.23559(5)
Os(3)	0.16713(8)	0.12099(8)	0.19572(5)
Os(4)	0.46295(8)	0.11734(8)	0.23030(6)
Os(5)	0.34697(8)	0.26363(7)	0.12157(5)
Os(6)	0.35073(8)	0.51335(8)	0.17015(5)
Pd(1)	0.2867(2)	0.2177(1)	0.3391(1)
O(11)	0.481(2)	0.594(2)	0.384(1)
O(12)	0.732(2)	0.436(2)	0.225(1)
O(13)	0.595(2)	0.270(2)	0.418(1)
O(21)	−0.047(2)	0.427(2)	0.123(1)
O(22)	−0.036(2)	0.297(1)	0.345(1)
O(23)	0.167(2)	0.600(1)	0.341(1)
O(31)	−0.039(2)	0.136(2)	0.061(1)
O(32)	−0.033(2)	0.037(2)	0.305(1)
O(33)	0.195(2)	−0.137(2)	0.131(1)
O(41)	0.748(2)	0.161(2)	0.195(1)
O(42)	0.550(2)	−0.003(2)	0.372(1)
O(43)	0.479(2)	−0.117(2)	0.126(1)
O(51)	0.334(2)	0.029(2)	0.012(1)
O(52)	0.612(2)	0.302(2)	0.047(1)
O(53)	0.160(2)	0.346(1)	−0.004(1)
O(61)	0.588(2)	0.576(2)	0.081(1)
O(62)	0.369(2)	0.754(2)	0.269(1)
O(63)	0.155(2)	0.607(2)	0.055(1)
N(1)	0.250(2)	0.314(2)	0.454(1)
N(2)	0.240(2)	0.081(2)	0.409(1)
C(1A)	0.193(2)	0.249(2)	0.504(1)
C(1B)	0.131(2)	0.298(2)	0.570(2)
C(1C)	0.136(2)	0.422(2)	0.586(2)
C(1D)	0.197(2)	0.490(2)	0.538(2)
C(1E)	0.255(2)	0.434(2)	0.473(1)
C(2A)	0.199(2)	0.120(2)	0.483(1)
C(2B)	0.167(2)	0.040(2)	0.536(2)
C(2C)	0.175(2)	−0.077(2)	0.513(2)
C(2D)	0.216(2)	−0.120(2)	0.439(2)
C(2E)	0.246(2)	−0.040(2)	0.388(1)
C(11)	0.469(2)	0.509(2)	0.339(2)
C(12)	0.626(2)	0.407(2)	0.241(2)
C(13)	0.534(2)	0.293(2)	0.359(2)
C(21)	0.039(2)	0.405(2)	0.165(1)
C(22)	0.054(2)	0.310(2)	0.305(1)
C(23)	0.177(2)	0.516(2)	0.297(1)
C(31)	0.039(2)	0.132(2)	0.114(1)
C(32)	0.047(2)	0.069(2)	0.265(1)
C(33)	0.191(2)	−0.037(2)	0.159(1)
C(41)	0.638(2)	0.143(2)	0.208(2)
C(42)	0.515(2)	0.043(2)	0.318(2)
C(43)	0.465(2)	−0.031(2)	0.168(1)
C(51)	0.338(2)	0.115(2)	0.059(1)
C(52)	0.510(2)	0.291(2)	0.077(2)
C(53)	0.230(2)	0.322(2)	0.045(1)
C(61)	0.495(2)	0.549(2)	0.115(1)
C(62)	0.363(2)	0.663(2)	0.230(1)
C(63)	0.228(2)	0.571(2)	0.100(1)
C(1)	0.178(2)	0.248(2)	0.813(2)
Cl(1)	0.0215(7)	0.2698(7)	0.7660(5)
Cl(2)	0.1747(7)	0.1235(6)	0.8620(5)
Cl(3)	0.2996(7)	0.2354(8)	0.7427(5)

eV, $\zeta(p) = 2.152$; $H_{ii}(d) = -12.02$ eV, $\zeta_1(d) = 5.983$ ($c_1 = 0.526$) and $\zeta_2(d) = 2.613$ ($c_2 = 0.6377$). The valence electron density and the molecular orbital wavefunctions were plotted with the use of the program MOPLOT [44].

3.8. X-ray data collection and structural determination of 1–4

All pertinent crystallographic data and other experimental details are summarized in Table 5. Data were collected at ambient temperature on an Enraf–Nonius CAD4-diffractometer (for **1**) or a Rigaku AFC7R diffractometer (for **2–4**), using Mo Kα radiation (λ = 0.71073 Å) with a graphite crystal monochromator in the incident beam. The unit-cell parameters were determined from a number of accurately centred reflections. The stability of the crystals was monitored at regular intervals using three standard reflections and no significant decay was observed. The diffracted intensities were corrected for Lorentz and polarization effects. Ψ scan method was employed for semiempirical absorption corrections [45]. Scattering factors were taken from [46a] and anomalous dispersion effects [46b] were included in F_c.

The structures were solved by direct methods MULTAN 80 [47], SIR 88 [48], SAPI 90 [49] and SAPI 91 [50] (see Table 5) and expanded by Fourier techniques. The solutions were refined on F by full-matrix least-squares analysis with Os, Pd, Cl and I atoms refined anisotropically. The hydrogen atoms of the chloroform (**1**), the bipyridine ligands (**1**, **3** and **4**) and the *n*-butyl groups (**2**) were generated in their ideal positions (C–H, 0.95 Å), while the metal hydrides for **4** were located on the difference Fourier map of the small-angle data and fixed without further refinement. All the hydrogen atoms were included but not refined. Calculations were performed on a MicroVax II (**1**) or a Silicon-Graphics (**2–4**) computer, using the program packages SDP (from Enraf–Nonius) [51] or TeXsan (from MSC) [52]. Positional parameters for the non-hydrogen atoms are given in Tables 6–9.

Table 7
Atomic coordinates for **2** with estimated standard deviations in parentheses

Atom	x	y	z
I(1)	0.0733(2)	0.2152(2)	0.9890(1)
I(2)	−0.0370(2)	0.3287(2)	0.8482(1)
I(3)	0.3023(2)	0.2470(2)	0.9451(1)
I(4)	0.1973(2)	0.3468(2)	0.8152(1)
I(5)	0.5381(2)	0.2660(2)	0.9098(1)
I(6)	0.4208(2)	0.3666(2)	0.7670(1)
Pd(1)	0.1296(2)	0.2840(2)	0.9004(1)
Pd(2)	0.3695(2)	0.3070(2)	0.8586(1)
N(1)	0.775(2)	0.050(2)	0.885(1)
N(2)	0.293(2)	0.434(2)	0.137(1)
C(1)	0.679(2)	0.002(2)	0.880(1)
C(2)	0.678(3)	−0.089(3)	0.911(1)
C(3)	0.578(3)	−0.125(3)	0.909(2)
C(4)	0.526(3)	−0.066(3)	0.944(2)
C(5)	0.823(2)	0.065(2)	0.946(1)
C(6)	0.767(3)	0.119(3)	0.981(2)
C(7)	0.820(3)	0.133(3)	1.041(2)
C(8)	0.764(3)	0.189(3)	1.078(2)
C(9)	0.839(3)	−0.013(3)	0.857(1)
C(10)	0.931(3)	0.027(3)	0.851(2)
C(11)	0.986(3)	−0.042(3)	0.827(2)
C(12)	1.080(3)	−0.003(3)	0.820(2)
C(13)	0.756(3)	0.138(3)	0.852(2)
C(14)	0.717(3)	0.135(3)	0.789(2)
C(15)	0.703(3)	0.237(3)	0.766(2)
C(16)	0.662(4)	0.242(4)	0.707(3)
C(17)	0.222(2)	0.360(2)	0.142(1)
C(18)	0.138(3)	0.387(3)	0.168(1)
C(19)	0.068(3)	0.307(3)	0.165(2)
C(20)	−0.016(3)	0.331(3)	0.193(2)
C(21)	0.335(2)	0.478(3)	0.195(1)
C(22)	0.385(3)	0.408(3)	0.237(2)
C(23)	0.412(3)	0.454(3)	0.296(2)
C(24)	0.329(3)	0.470(3)	0.324(2)
C(25)	0.369(2)	0.387(2)	0.111(1)
C(26)	0.453(2)	0.446(3)	0.103(1)
C(27)	0.518(3)	0.391(3)	0.074(1)
C(28)	0.604(3)	0.446(3)	0.069(2)
C(29)	0.249(2)	0.516(3)	0.100(1)
C(30)	0.203(3)	0.490(3)	0.039(2)
C(31)	0.168(3)	0.580(3)	0.010(2)
C(32)	0.108(4)	0.558(4)	−0.051(2)

Table 8
Atomic coordinates for **3** with estimated standard deviations in parentheses

Atom	x	y	z
Os(1)	0.15362(2)	−0.00168(2)	0.21257(5)
Os(2)	0.1250	0.06020(2)	0.1250
Pd(1)	0.12905(5)	−0.06754(3)	0.23499(9)
O(1)	0.2242(4)	−0.0567(3)	0.2388(8)
O(2)	0.0656(4)	−0.0177(3)	0.3266(8)
O(3)	0.2377(4)	0.0147(3)	0.0900(8)
O(4)	0.1835(4)	0.0324(3)	0.3976(10)
O(5)	0.1901(5)	0.1072(3)	0.2338(10)
O(6)	0.0651(4)	0.0582(3)	0.3103(9)
N(1)	0.1489(4)	−0.1203(3)	0.2481(9)
N(2)	0.0636(4)	−0.0960(3)	0.2426(9)
C(1)	0.1881(6)	−0.0450(4)	0.231(1)
C(2)	0.0980(6)	−0.0153(4)	0.278(1)
C(3)	0.2066(5)	0.0098(4)	0.135(1)
C(4)	0.1750(6)	0.0188(4)	0.325(1)
C(5)	0.1642(6)	0.0893(4)	0.191(1)
C(6)	0.0854(6)	0.0573(4)	0.239(1)
C(7)	0.1144(6)	−0.1426(4)	0.253(1)
C(8)	0.1233(7)	−0.1784(4)	0.262(1)
C(9)	0.1684(6)	−0.1880(5)	0.266(1)
C(10)	0.2018(6)	−0.1652(5)	0.261(1)
C(11)	0.1911(6)	−0.1309(4)	0.252(1)
C(12)	0.0684(5)	−0.1306(4)	0.249(1)
C(13)	0.0301(7)	−0.1507(5)	0.248(1)
C(14)	−0.0103(7)	−0.1380(5)	0.239(1)
C(15)	−0.0153(7)	−0.1023(5)	0.231(1)
C(16)	0.0229(6)	−0.0830(4)	0.235(1)

Table 9
Atomic coordinates for **4** with estimated standard deviations in parentheses

Atom	x	y	z
Os(1)	0.63834(8)	0.21762(6)	1.2582(1)
Os(2)	0.67253(8)	0.09493(6)	0.9977(1)
Os(3)	0.76498(8)	0.07212(6)	1.3441(1)
Os(4)	0.83574(8)	0.16163(6)	1.1579(1)
Pd(1)	0.0991(1)	0.4458(1)	0.4104(2)
Pd(2)	−0.0451(1)	0.5270(1)	0.1902(2)
O(1)	0.679(1)	0.321(1)	1.574(2)
O(2)	0.437(2)	0.213(1)	1.339(2)
O(3)	0.546(1)	0.345(1)	1.039(2)
O(4)	0.582(1)	0.207(1)	0.741(2)
O(5)	0.732(2)	−0.051(1)	0.748(3)
O(6)	0.457(2)	0.091(1)	1.014(3)
O(7)	0.923(1)	−0.084(1)	1.416(2)
O(8)	0.583(2)	0.047(1)	1.447(3)
O(9)	0.831(1)	0.153(1)	1.676(2)
O(10)	0.905(2)	0.259(1)	1.461(3)
O(11)	0.776(1)	0.2962(9)	0.955(2)
O(12)	1.043(2)	0.078(1)	1.026(3)
O(13)	−0.048(1)	0.3730(9)	0.217(2)
N(1)	0.234(1)	0.465(1)	0.566(2)
N(2)	0.178(1)	0.337(1)	0.497(2)
N(3)	−0.081(1)	0.6400(10)	0.117(2)
N(4)	−0.174(1)	0.532(1)	0.013(2)
C(1)	0.659(2)	0.280(1)	1.450(3)
C(2)	0.516(2)	0.215(1)	1.317(3)
C(3)	0.578(2)	0.296(1)	1.121(3)
C(4)	0.616(2)	0.165(1)	0.838(3)
C(5)	0.712(2)	0.004(2)	0.843(3)
C(6)	0.544(2)	0.090(2)	1.012(3)
C(7)	0.860(2)	−0.025(1)	1.381(3)
C(8)	0.651(2)	0.057(1)	1.410(3)
C(9)	0.803(2)	0.122(2)	1.548(4)
C(10)	0.885(2)	0.219(2)	1.347(3)
C(11)	0.802(2)	0.245(1)	1.034(3)
C(12)	0.966(2)	0.109(2)	1.084(4)
C(13)	−0.012(2)	0.424(1)	0.255(3)
C(14)	0.252(2)	0.531(1)	0.599(3)
C(15)	0.345(2)	0.538(2)	0.684(3)
C(16)	0.412(2)	0.475(2)	0.750(4)
C(17)	0.393(2)	0.403(2)	0.722(4)
C(18)	0.301(2)	0.402(1)	0.637(3)
C(19)	0.266(2)	0.332(1)	0.596(3)
C(20)	0.322(2)	0.267(2)	0.674(3)
C(21)	0.291(2)	0.202(2)	0.626(4)
C(22)	0.202(2)	0.204(2)	0.527(3)
C(23)	0.149(2)	0.274(2)	0.461(3)
C(24)	−0.027(2)	0.690(1)	0.173(3)
C(25)	−0.054(2)	0.763(2)	0.123(3)
C(26)	−0.142(2)	0.785(1)	0.011(3)
C(27)	−0.203(2)	0.734(1)	−0.049(3)
C(28)	−0.168(2)	0.660(1)	0.009(3)
C(29)	−0.220(2)	0.603(1)	−0.049(3)
C(30)	−0.302(2)	0.611(1)	−0.168(3)
C(31)	−0.344(2)	0.556(1)	−0.223(3)
C(32)	−0.300(2)	0.486(1)	−0.165(3)
C(33)	−0.215(2)	0.475(1)	−0.041(3)

Tables of hydrogen atom coordinates and thermal parameters and complete lists of bond lengths and angles have been deposited at the Cambridge Crystallographic Data Centre.

Acknowledgements

This work is funded by the Croucher Foundation and the University of Hong Kong. S.C. thanks the Croucher Foundation for financial support.

References

[1] R.D. Adams and W. Wu, *Organometallics*, 12 (1993) 1248, and references cited therein.
[2] R.D. Adams, J.E. Babin, R. Mathab and S. Wang, *Inorg. Chem., 25* (1986) 1623, and references cited therein.
[3] C. Couture and D.H. Farrar, *J. Chem. Soc., Dalton Trans.*, (1987) 2245, 2253.
[4] L.J. Farrugia, J.A.K. Howard, P. Mitrprachachon, J.L. Spencer, F.G.A. Stone and P. Woodward, *J. Chem. Soc., Dalton Trans.*, (1981) 171.
[5] L.J. Farrugia, J.A.K. Howard, P. Mitrprachachon, F.G.A. Stone and P. Woodward, *J. Chem. Soc., Dalton Trans.*, (1981) 155, 162, 171.
[6] E. Brivio, A. Ceriotti, R.D. Perogola, L. Garlaschelli, F. Demartin, M. Manassero, M. Sansoni, P. Zanello, F. Laschi and B.T. Heaton, *J. Chem. Soc., Dalton Trans.*, (1994) 3237.
[7] R.D. Adams, J.-C. Lii and W. Wu, *Inorg. Chem., 31* (1992) 2556.
[8] S. Chan and W.-T. Wong, *J. Chem. Soc., Dalton Trans.*, (1994) 1605.
[9] S. Chan and W.-T. Wong, *J. Organomet. Chem., 489* (1995) C78.
[10] R.J. Goudsmit, J.G. Jeffrey, B.F.G. Johnson, J. Lewis, R.C.S. McQueen, A.J. Sanders and J.-C. Liu, *J. Chem. Soc., Chem. Commun.*, (1986) 24.
[11] C.R. Eady, B.F.G. Johnson and J. Lewis, *J. Chem. Soc., Dalton Trans.*, (1975) 2606.
[12] A.J. Amoroso, B.F.G. Johnson, J. Lewis, C.K. Li, C.A. Morewood, P.R. Raithby, M.D. Vargas and W.T. Wong, *J. Cluster Sci., 6* (1995) 163.
[13] R. Goddard, P.W. Jolly, C. Krüger, K.-P. Schick and G. Wilke, *Organometallics, 1* (1982) 1709.
[14] R.D. Pergola, F. Demartin, L. Garlaschelli, M. Manassero, S. Martinengo, N. Masciocchi and M. Sansoni, *Organometallics, 10* (1991) 2239.
[15] R.D. Pergola, L. Garlaschelli, F. Demartin, M. Manassero and N. Masciocchi, *J. Organomet. Chem., 436* (1992) 241.
[16] B.F.G. Johnson, J. Lewis, W.J.H. Nelson, P. Puga, P.R. Raithby, D. Braga, M. McPartlin and W. Clegg, *J. Organomet. Chem., 243* (1983) C13.
[17] A. Fumagalli, G. Longoni, P. Chini, A. Albinati and S. Bruckner, *J. Organomet. Chem., 202* (1980) 329.
[18] D.M.P. Mingos, *Acc. Chem. Res., 17* (1984) 311.
[19] D.M.P. Mingos, *J. Chem. Soc., Chem. Commun.*, (1983) 706.
[20] W.-T. Wong, personal communication, 1989.
[21] M.I. Bruce and B.K. Nicholson, *Organometallics, 3* (1984) 101.
[22] J.A.K. Howard, I.D. Salter and F.G.A. Stone, *Polyhedron, 3* (1984) 567.
[23] F. Maassarani, M. Pfeffer and G. Le Borgne, *J. Chem. Soc., Chem Commun.*, (1987) 565.
[24] F. Maassarani, M. Pfeffer and G. Le Borgne, *Organometallics, 6* (1987) 2029.
[25] D.F. Shriver, H.D. Kaesz and R.D. Adams, *The Chemistry of Metal Cluster Complexes*, VCH, Weinheim, 1990, p. 34.
[26] E. Sappa, A. Tiripicchio and P. Braunstein, *Coord. Chem. Rev., 65* (1985) 219.

[27] F.A. Cotton, *Prog. Inorg. Chem., 21* (1976) 1.
[28] E.M. McGhee, B.M. Hoffman and J.A. Ibers, *Inorg. Chem., 30* (1991) 2162.
[29] J.-M. Barbe, P. Richard, M.A. Aukauloo, C. Lecomte, P. Petit and R. Guilard, *J. Chem. Soc., Chem. Commun.*, (1994) 2757.
[30] C.A. Hunter, *Angew. Chem., Int. Edn. Engl., 32* (1993) 1584.
[31] Z. Lin and M.B. Hall, *Inorg. Chem., 30* (1991) 2569.
[32] V.N. Zudin, V.D. Chinakov, V.M. Nekipelov, V.A. Likholobov and Y.I. Yermakov, *J. Organomet. Chem., 289* (1985) 425.
[33] A.R. Siedle, R.A. Newmark and W.B. Gleason, *Inorg. Chem., 30* (1991) 2005.
[34] M. Portnoy, F. Frolow and D. Milstein, *Organometallics, 10* (1991) 3960.
[35] M. Portnoy and D. Milstein, *Oganometallics, 13* (1994) 600.
[36] G. Minghetti, A.L. Bandini, G. Banditelli, F. Bonati, R. Szostak, C.E. Strouse, C.B. Knobler and H.D. Kaesz, *Inorg. Chem., 22* (1983) 2332.
[37] J.-C. Tsai, M.A. Khan and K.M. Nicholas, *Organometallics, 10* (1991) 29; J.-C. Tsai, R.A. Wheeler, M.A. Khan and K.M. Nicholas, *Organometallics, 10* (1991) 1344.
[38] (a) J.N. Nicholls and M.D. Vargas, *Inorg. Synth., 28* (1990) 234; (b) J.N. Nicholls and M.D. Vargas, *Inorg. Synth., 28* (1990) 238; (c) J.N. Nicholls and M.D. Vargas, *Inorg. Synth., 26* (1989) 295.
[39] G.D. Smith, B.E. Hanson, J.S. Merola and F.J. Walles, *Organometallics, 12* (1993) 568.
[40] B.F.G. Johnson, J. Lewis, P.R. Raithby, G.M. Sheldrick and K. Wong, *J. Chem. Soc., Dalton Trans.*, (1978) 673
[41] (a) M.B. Hall and R.F. Fenske, *Inorg. Chem., 11* (1972) 768; (b) A.L. Sargent and M.B. Hall, *Polyhedron, 9* (1990) 1977.
[42] (a) R. Hoffmann, *J. Chem. Phys., 39* (1963) 1397; (b) R. Hoffmann and W.N. Lipscomb, *J. Chem. Phys., 36* (1962) 2179, 3189; *37* (1962) 2872.
[43] R.H. Summerville and R. Hoffmann, *J. Am. Chem. Soc., 98* (1976) 7240.
[44] Interactive MOPLOT: a package for the interactive display and analysis of molecular wavefunctions incorporating the program MOPLOT (D. Lichtenburger), PLOTDEN (R.F.W. Bader, D.J. Kenworthy, P.M. Beddal, G.R. Runtz and S.G. Anderson), SCHUSS (R.F.W. Bader, G.R. Runtz, S.G. Anderson and F.W. Biegler-Koenig) and EXTREM (R.F.W. Bader and F.W. Biegler-Koenig), P. Sherwood and P.J. MacDougall, 1989.
[45] A.C.T. North, D.C. Phillips and F.S. Mathews, *Acta Crystallogr., Sect. A, 24* (1968) 351.
[46] (a) D.T. Cromer and J.T. Waber, *International Tables for X-ray Crystallography*, Vol. 4, Kynoch, Birmingham, 1974, Table 2.2B; (b) D.T. Cromer and J.T. Waber, *International Tables for X-ray Crystallography*, Vol. 4, Kynoch, Birmingham, 1974, Table 2.3.1.
[47] P. Main, S.J. Fiske, S.E. Hill, L. Lessinger, G. Germain, J.-P. Declercq and M.M. Wolfcon, *MULTAN 80, A System of Computer Programs for the Automatic Solution of Crystal Structures from X-ray Diffraction Data*, University of York, York, University of Louvain, Louvain, 1980.
[48] M.C. Burla, M. Camalli, G. Cascarano, C. Giacovazzo, G. Polidor, R. Spagna and D. Viterbo, *J. Appl. Crystallogr., 22* (1989) 389.
[49] H.-F. Fan, *Structure Analysis Programs with Intelligent Control*, Rigaku Corporation, Tokyo, 1990.
[50] H.-F. Fan, *Structure Analysis Programs with Intelligent Control*, Rigaku Corporation, Tokyo, 1991.
[51] *SDP Structure Determination Package*, Enraf–Nonius, Delft, 1985.
[52] *TeXsan: Crystal Structure Analysis Package*, Molecular Structure Corporation, 1985, 1992.